American Mineralogist, Volume 84, pages 895–904, 1999

In situ study of the goethite-hematite phase transformation by real time synchrotron powder diffraction

ALESSANDRO F. GUALTIERI* AND PAOLO VENTURELLI

Dipartimento di Scienze della Terra, Università di Modena I-41100 Modena, Italy

ABSTRACT

The temperature induced goethite-hematite phase transformation that occurs at about 250 °C was studied using in situ synchrotron X-ray powder diffraction with a capillary Debye-Scherrer geometry and a translating image plate system (TIPS). To our knowledge, this is the first time the goethite-hematite transformation has been investigated in real time. The sample was a pure, synthetic, stoichiometric goethite with 1 μm long needle-shaped crystals. The microstructural characterization showed that the sample was well crystallized. The Rietveld refinement of 30 powder patterns extracted from the image in the range 25–800 °C demonstrates that an intermediate phase with non-stoichiometric composition (*"protohematite"*) forms after the decomposition of goethite. The cell parameter *b* of goethite dramatically decreased during the phase transformation while *a* and *c* instead continued to increase. Protohematite is iron-deficient and retains residual hydroxyls for charge balance. With temperature protohematite progressively transforms into hematite. Empty layers (pores) are consequently formed about the hematite clusters. The distribution of iron vacancies was modeled in the powder patterns with stacking faults that were simulated using anisotropic broadening coefficients of the pseudo-Voigt profile function. Its disappearance with temperature was effectively followed with a decrease of the density of stacking faults.

INTRODUCTION

Goethite and hematite are the main Fe-bearing minerals in sedimentary red beds. Hematite is abundant in ancient red beds whereas goethite is abundant in younger yellow-brown colored deposits. It is generally accepted that hematite is a post-depositional phase formed during diagenesis (Goss 1987). The origin of hematite is still unclear. Several origins have been proposed including in situ formation of red hematitic soil; aging of amorphous limonite; dehydration of crystalline goethite; and dissolution of original goethite and re-precipitation of an intermediate ferrihydrate phase (Goss 1987). Thus, the goethite-hematite phase transformation has a paramount importance for the understanding of diagenetic processes in sedimentary red beds.

Goethite, α-FeOOH is commonly described in the orthorhombic space group *Pbnm* with $a = 4.587$ Å, $b = 9.937$ Å, and $c = 3.015$ Å (Lima-De-Faria 1963). In this work, the orthorhombic space group *Pnma* having $a = 9.95$ Å, $b = 3.01$ Å, $c = 4.62$ Å ($Z = 4$) (Szytuta et al. 1968) was used because the unit cell could be easily compared to the one of hematite in which the *c* axis is coincident and three times the *c* axis of goethite. The structure of goethite is based on an arrangement of O atoms in an hexagonal close packing, with Fe^{3+} ions occupying half of the octahedral sites (Fig. 1). Hematite, α-Fe_2O_3, is rhombohedral, space group $R\bar{3}c$ with hexagonal cell constants $a = b = 5.038$ Å, $c = 13.772$ Å, $Z = 6$ (Blake et al. 1966). The framework of hematite is regarded as a set of O and Fe layers, arranged normal to the threefold axis. Anions are arranged in an hexagonally close packing, with minor distortions, so that Fe^{3+} atoms occupy two-thirds of the octahedral interstices (Fig. 1).

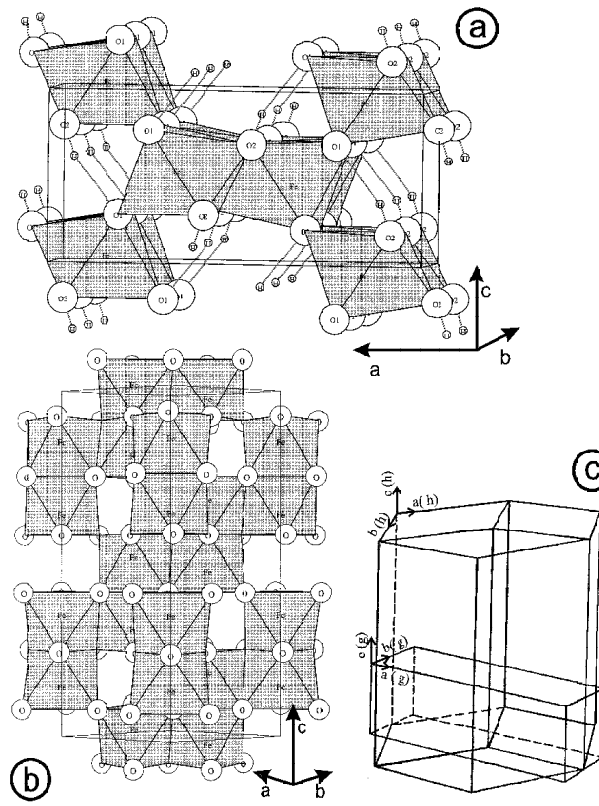

FIGURE 1. The structure of **(a)** goethite, **(b)** hematite, and **(c)** cell relationship.

*E-mail: alex@unimo.it

The goethite-hematite phase transformation has been widely investigated. Goldsztaub (1931) defined it as *pseudomorfic*; Bernal et al. (1958) regarded this transformation among those known as *topotattic* to indicate solid-state transformations where close structural relationships between the two transforming phases are preserved. Rooksby (1951) observed a non-uniform broadening of the powder diffraction peaks of hematite formed from heated goethite. He postulated that this effect was due to a particular shape of the crystallites of the original goethite. Francombe and Rooksby (1959) observed unit-cell relationships between goethite and hematite (Fig. 1). The unit cells of goethite and hematite can be regarded as representative of two types of superlattice, produced by ordering of iron ions in different ways in the basic O framework.

Lima De Faria (1963) observed the appearance of satellites next to main diffraction spots in heated natural goethite single crystals and suggested the existence of a modulation of the structure along the *c* axis with an amplitude of 32 Å. He postulated that during the transformation from goethite to hematite two different Fe distributions are possible. The probability of nucleation of each of these two forms is the same and this should yield domains of the two in twin relationships. He also observed an intermediate state of the transformation with a selective broadening of certain diffraction peaks, ascribed to the presence of stacking faults.

Watari et al. (1979a) studied this transformation using high-resolution transmission electron microscopy (TEM) and demonstrated the presence of twins. These authors saw two types of monodimensional fringes produced by the presence of two sets of twins and proposed that satellite spots are due to textural effects, rather than to the existence of a superstructure (the reaction must occur directly, without any intermediate state). Watari et al. (1983) suggested that the reaction occurs first at the surface of goethite by producing a layer of twinned crystals of hematite and proceeds inward with the formation of voids. Besides, they supposed that the transformation reaction is strongly affected by many factors such as grain size, heating rate, nature, and preparation of sample.

Goss (1987) observed that the reaction starts from the surface of goethite grains, with the formation of lattice fringes in TEM images. These structures where interpreted as elongated and parallel pores, developed from the surface inward during the dehydration of goethite. Wolska (1981) and Wolska and Schwertmann (1989) interpreted this phase transformation with a mechanism involving the presence of an intermediate phase, called *protohematite*. Through IR spectroscopy they showed how hematite derived from goethite retains hydroxyls and a lack of iron with respect to stoichiometric hematite. They proposed for this phase the following chemical formula: α-$Fe_{2-x/3}(OH)_xO_{3-x}$ with x = number of residual hydroxyls in the structure.

The iron deficiency was detected by measurement of the integrated intensities of certain powder peaks. In the final stage of the process they observed the complete disappearance of OH and the achievement of the stoichiometry of hematite.

Many points regarding the goethite-hematite phase transformation are still unclear and debated. All the reported data on the phase transformation are from ex situ experiments. The major issues are (1) the role of protons during the phase transformation and stoichiometry of the forming hematite (does a non-stoichiometric intermediate phase really exist after the phase transformation?); (2) the non-ubiquitous formation of hematite twins after the phase transformation; (3) the presence and role of stacking disorder in forming intermediate phase; and (4) the presence and role at higher temperature of pores intercalated within the layers of hematite to form a peculiar *texture*. To shed light on these points, the phase transformation was investigated for the first time in real time using in situ synchrotron powder diffraction. Rietveld refinement was performed on 30 patterns in the temperature range 25–800 °C. The very good quality of the data allowed refinement of H positions as well as Fe and O.

EXPERIMENTAL METHODS

Materials and ancillary experiments

The goethite sample was a pure, synthetic material produced by Bayer. The synthesis method is based on high-temperature oxidation and hydrolysis in air of an Fe-sulfate, in the presence of metallic iron. Grain size distribution of the sample was determined by laser granulometry carried out with a Fritsch Analysette 22 device. This sample was also investigated by scanning electon microscopy (SEM), using a Philips XL40/604 device. Preliminary powder diffraction patterns were collected on a Philips PW3710 automated diffractometer with copper anode (Cu$K\alpha$ = 1.5418 Å), parafocusing Bragg-Brentano geometry, flat specimen, and gas-proportional counter. Determination of crystal mean size followed the methodology described in Young and Wiles (1982), Louër and Langford (1988), Langford et al. (1993), and Van Berkum et al. (1996). The profile function of a powder pattern is assumed to be the convolution of the instrumental and microstructural broadening, according to the relation $f(2\theta) = g(2\theta)\cdot h(2\theta)$, with $g(2\theta)$ = microstructural function, and $h(2\theta)$ = instrumental function. For the calculation of the microstructural broadening it is necessary to deconvolute the instrumental contribution. To this aim, we collected the powder pattern of BaF_2 produced by Merck (suprapur quality) annealed following the procedure described in Louër and Langford (1988). The standard powder pattern was used for calculation of the integral breadth of the peaks of BaF_2 vs. 2θ.

For the fitting of the full width at half maximum (FWHM) of the peaks we utilized the equation proposed by Louër and Langford (1988):

$$(\text{FWHM})^2 = \text{Atan}^2(\theta)+\text{B}+\text{Ccotan}^2(\theta) \quad (1)$$

This relation was then used for the deconvolution of the instrumental contribution from the FWHM values of goethite. The goethite FWHMs, cleared from instrumental contribution, were employed for the calculation of the grain size and microstrain using the equations:

$$D = \lambda/[(LX_g - LX_s \quad (2)$$

$$e = (GU_g - GU_{st})/4\tan(\theta) \quad (3)$$

where g = goethite, st = BaF_2. The profile coefficients LX and GU are parameters of the Lorentzian [$\gamma = (\text{LX})\tan(\theta)+(\text{LY})/(\cos\theta)+\text{Z}$] and Gaussian

$$\sigma^2 = (\text{GU})\tan^2(\theta) + \text{GV}\tan(\theta) + GW + \frac{P}{\cos^2(\theta)}$$

broadening in the pseudo-Voigt function and were calculated using GSAS (Cagliotti et al. 1958; Larson and Von Dreele 1998). Thermal analyses were carried out with a SEIKO ssc/5200 from room temperature (RT) to 1000 °C, with an heating rate of 13 °C/min up to 90 °C, and 2 °C/min from 90 to 1000 °C.

Real time synchrotron diffraction

The phase transformation was followed by real time synchrotron powder diffraction at the X7B beam line of the National Synchrotron Light Source (Brookhaven National Laboratory, U.S.A.), with a Huber four circle diffractometer. The X7B beamline geometry is described in detail in Hastings et al. (1983). The powder sample was mounted in a rotating capillary, on a standard goniometer head. The heating system was a hot air flow created by a heating gun device with a maximum heating temperature of 800 °C. The temperature was controlled by a thermocouple positioned at about 1 mm below the specimen. The experiment was performed using a fixed λ of 0.9602 Å. A 3 mm wide cross section of the diffracted rings was recorded on an image plate (IP) detector (Amemija 1990), mounted on a translating system called translating image plate system (TIPS) (Norby 1997). The IP detector is mounted on a slide behind a steel screen with a vertical 3 mm wide slit and the heating rate of the experiment was synchronized with the speed of the slide to record the continuous change of the diffracted rings with temperature (Fig. 2). The heating rate was the same used for the thermal analysis. The image stored in the IP was then recovered using a Fuji BAS2000 scanner through a He-Ne laser simulation. The extraction of the powder patterns from the image was possible using an original code described in Gualtieri et al. (1996) and a continuous series of powder patterns was obtained in the range 25–800 °C. Raw data were corrected for the zero shift error, Lorentz polarization, and tilting angle a of the IP. Each powder pattern was refined using the GSAS program (Larson and Von Dreele 1998). The structure factors were calculated using scattering factors of atoms with formal charge, the background was fitted with a Chebyshev function with 24 coefficients, necessary to model increased background due to the glass capillary. Peak profiles were modeled using a pseudo-Voight function with GU, GW, LX, LY, and the lorentzian anisotropic broadening coefficients ptec[(LX+LX$_s$cosφ)tan(θ)] and sfec[(LY+LY$_s$cosφ)/(cosθ)] simulating a planar disorder along *c*, where φ = angle between the vector normal to the plane that contains stacking fauls and the diffusion vector (Larson and Von Dreele 1998). The lattice constants and the phase fraction were constantly refined. Atomic coordinates, populations, and thermal parameters were refined in the later stages of the refinement. Soft constraints on the O-H distances were imposed in goethite, and the population of H in hematite was restrained to the population of the Fe atoms, using the ideal composition in Wolska and Schwertmann (1989) (see further details in the results and discussion). The total number of parameters refined at the same time in the last stages of each refinement was 44 for spectra with goethite only, 63 for spectra with goethite plus hematite, and 44 for spectra with hematite only.

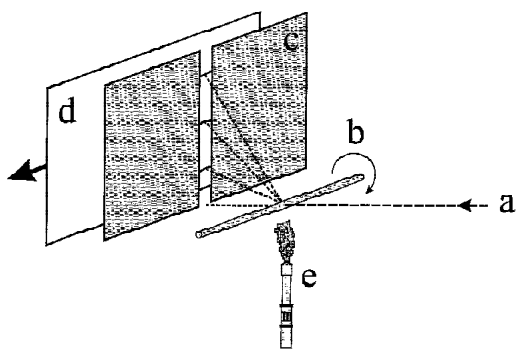

FIGURE 2. The experimental set-up for the real time experiments at X7B: **(a)** synchrotron beam; **(b)** rotating capillary; **(c)** aluminum slides in front of the IP; **(d)** translating IP system; and **(e)** heating gun.

TABLE 1. Results of the microstructure analysis

Peaks	θ	GU_g	Lx_g	LX_g	*D* (Å)	*e*
(110)	10.61	0.1	13	6.2	2528	4.7
(120)	13.16	3.9	10.5	3.7	4276	228

Note: [D(Å)] is the crystallite size; *e* is microstrain of goethite along the (110) and (120) directions.

RESULTS

SEM observation and grain size distribution showed that the goethite sample had an acicular morphology with 1 μm long needles. Table 1 reports the results of the microstructure analysis showing the dimension and microstrain of goethite along the (110) and (120) directions. The thermal analysis showed a total weight loss of 13.5%. DTA exhibits a doubled peak in correspondence with the dehydration process and a linear decrease of weight until 1000 °C (Fig. 3). Figure 4a reports the image obtained from the IP and relative three-dimensional plots are reported in Figure 4b. The reaction was followed by observing the disappearance of the goethite peaks and the growth of those of hematite. Powder patterns extracted from the digitalized image on the IP were refined with GSAS and agreement factors were excellent (*wRp* in the range 0.0361–0.0469 and χ^2 in the range 2.825–5.406, respectively). Some selected XRD observed and calculated patterns together with the difference curves are depicted in Figure 5 and testify of the

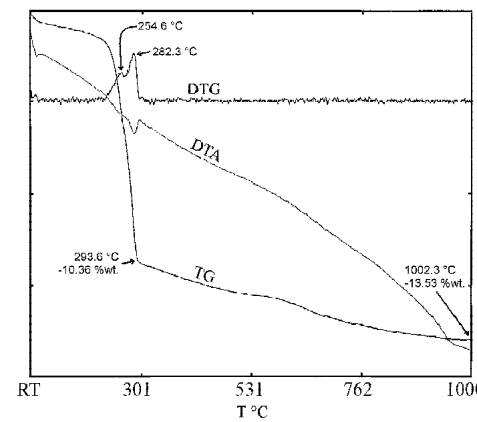

FIGURE 3. DTA, TG, and DTG analyses of the investigated sample.

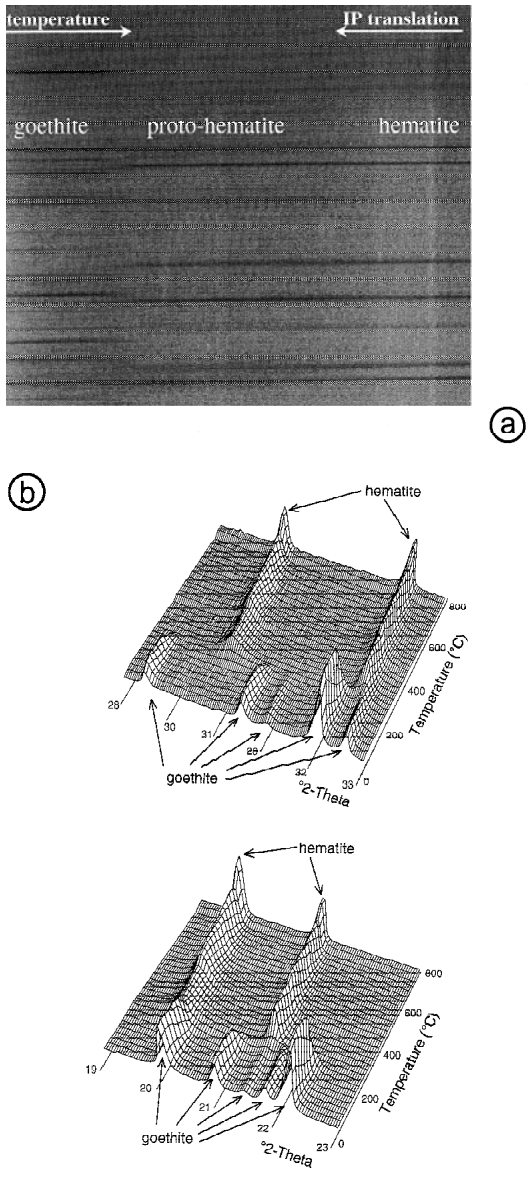

FIGURE 4. The image obtained from the IP **(a)** and three-dimensional plots (2θ-temperature-intensity) extracted by integration in the direction normal to the IP translation **(b)**. The 19–23 and the 28–33 ° 2θ regions are reported.

good fit of the data for either goethite and hematite.

Profile function parameters vs. temperature are illustrated in Figure 6a for goethite and in Figures 6b and 6c for hematite. The profile function of goethite was rather constant up to the phase transformation. Concerning hematite, the LX and LY drop is caused by a rise of newly formed hematite diffracting domains. The increase in GW is probably an artifact due to a correlation with LX. The *ptec* and *sfec* parameters were refined to account for the anisotropic broadening of the hematite peaks that was likely due to planar defectiveness decreasing with temperature (see discussion below). Figure 7a reports the evolution of the goethite unit cell with temperature. Hematite unit cells with temperature are instead depicted in Figure 7b; an increase of *a* and *c* due to thermal expansion is observed. The comparison of the cell volumes vs. temperature is reported in Figure 7c. Regarding the atomic populations in goethite, no

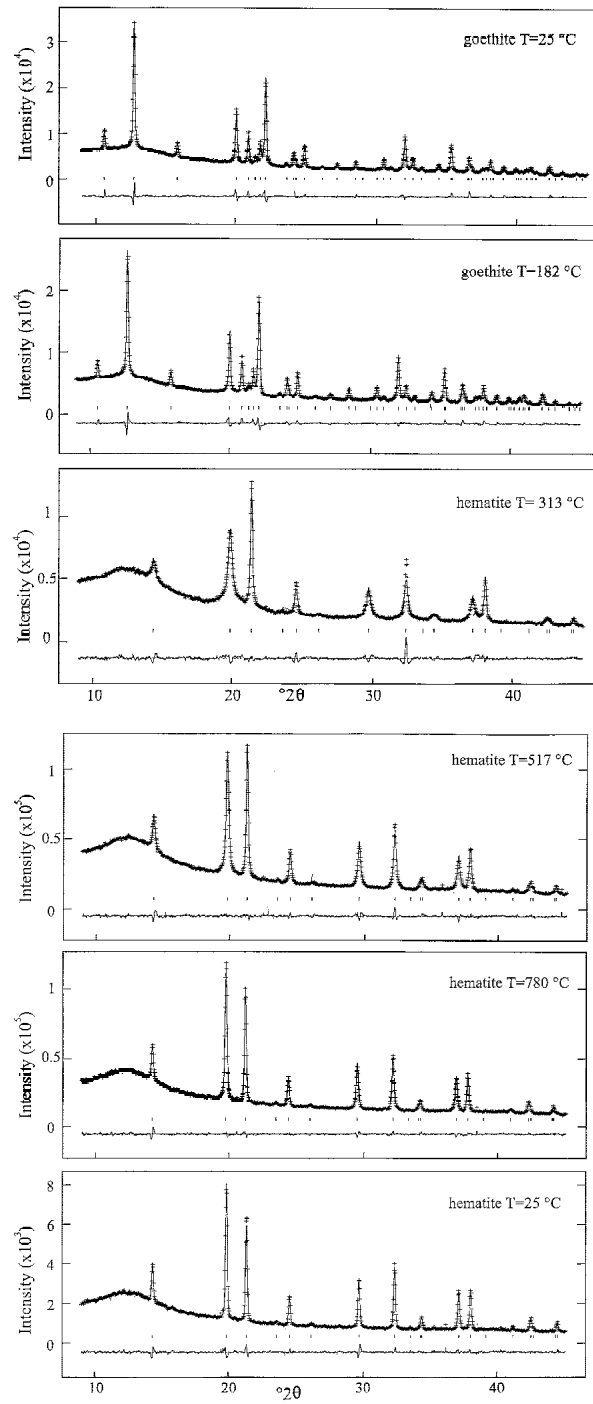

FIGURE 5. Observed, calculated powder patterns, and difference curve for some selected Rietveld refinements in the range 25–800 °C. At T = 25 °C and 182 °C with only goethite, at 313 °C, 517 °C, 780 °C, and after cooling at 25 °C with only hematite.

deviations from the stoichiometry was observed near the phase transformation. Hematite formed just after the phase transformation has a deficiency of iron atoms and an excess of residual hydroxyls. The changes of iron and hydrogen populations are depicted in Figure 8. Total hydrogen was calculated assuming the chemical restraint imposed by the chemical formula $Fe_{2-x/3}(OH)_xO_{3-x} \equiv Fe_{2-x/3}H_xO_3$.

The position of the residual hydrogen atom in hematite was calculated by considering the orientation relationship between the unit cells of goethite and hematite and the relative transformation matrix of the unit cell of goethite cell into the unit cell of hematite. Knowing the coordinates (X_g; Y_g; Z_g) of the H atom in goethite, the position of the H atom in the cell of hematite (X_h; Y_h; Z_h) were calculated using the following transformation matrix:

$$[X_g\ Y_g\ Z_g] \times \begin{bmatrix} 2 & 0 & 0 \\ \sqrt{3} & \sqrt{3} & 0 \\ 0 & 0 & 1/3 \end{bmatrix} = [X_h\ Y_h\ Z_h]$$

The so-obtained hydrogen atomic position was subsequently refined in a general position with multeplicity 36. Table 2 reports the results of some selected refinements in the range 25–800 °C.

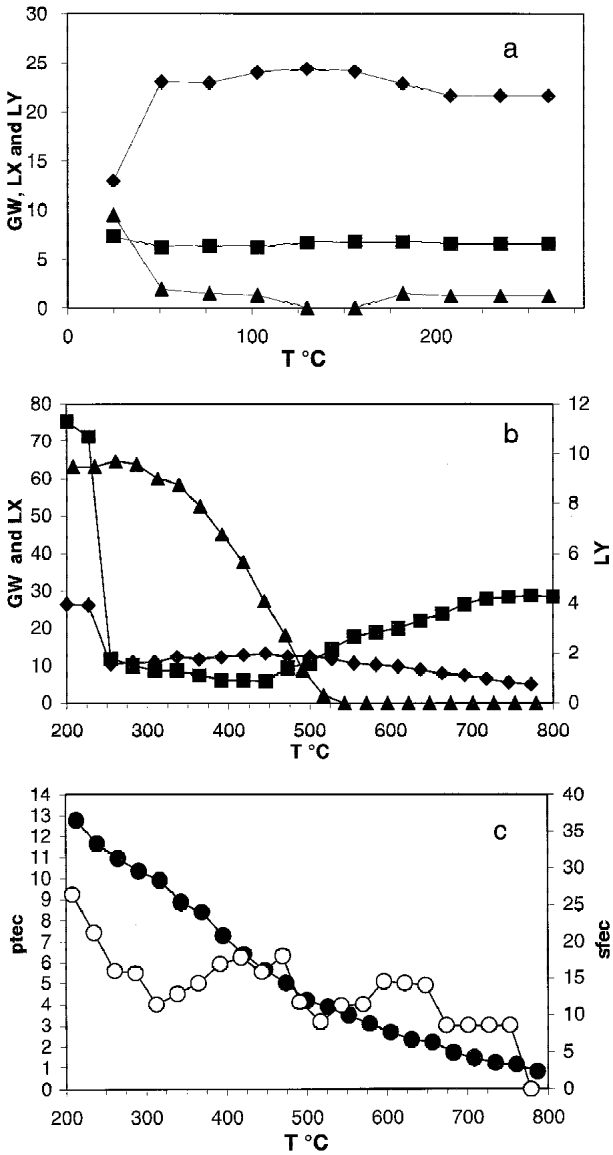

FIGURE 6. Refined profile function parameters vs. temperature for **(a)** goethite and for **(b)** and **(c)** hematite . Full rhombs = GW; full squares = LX; full triangles = LY; full circles = sfec; empty circles = ptec. Standard deviations are smaller than drawn points.

DISCUSSION

The microstructure characterization showed that the goethite sample is well crystallized. This is also seen by the comparison of the FWHM of the (110) reflection not corrected for the instrumental broadening ($2\theta = 0.10°$) with the corresponding values reported by Wolska and Schwertmann (1989) in their Table 1 (all the values are within $2\theta = 0.31$ and 1.64°). The refinement of the structure at 25 °C showed that the sample was stoichiometric FeOOH because a tentative refinement of hydrogen population yielded a value very close to 100%. This sample seemed an exception among natural goethites because according to Wolska and Schwertmann (1989) "…stoichiometric goethite is practically non existent…" In concert with this difference were the lower values of the water content and unit-cell constants of our sample. In particular, *b* and *c* were markedly lower albeit the values were not directly comparable because Wolska and Schwertmann (1989) did not make use of an internal standard for absolute reference. The thermal analysis showed that our sample had an excess of water (likely surface adsorbed water) that is lost at approximately 70 °C. If the value of the water lost at low temperature was subtracted to the total

TABLE 2. Results of selected Rietveld refinements at various temperatures.

	x/a	*y*/b	*z*/c	atoms per unit cell	U_{iso}
			***T* = 25 °C (goethite)**		
Fe	0.1459(1)	0.25	–0.0486(2)	4	0.049(5)
O1	–0.1990(4)	0.25	0.285(1)	4	0.046(5)
O2	–0.0517(4)	0.25	–0.196(1)	4	0.046(5)
H	–0.101(4)	0.25	–0.399(6)	4	0.06†
			***T* = 156 °C (goethite)**		
Fe	0.1459(1)	0.25	–0.0489(2)	4	0.048(5)
O1	–0.1994(4)	0.25	0.286(1)	4	0.050(5)
O2	–0.0499(5)	0.25	–0.209(1)	4	0.050(5)
H	–0.105(4)	0.25	–0.411(5)	4	0.06†
			***T* = 313 °C (hematite)**		
Fe	0	0	0.3531(1)	10.58(6)	0.053(5)
O	0.316(1)	0	0.25	18	0.054(5)
H	–0.20(3)	0.322(2)	–0.136(4)	0.42(6)*	0.06†
			***T* = 517 °C (hematite)**		
Fe	0	0	0.3537(1)	11.41(4)	0.059(5)
O	0.323(1)	0	0.25	18	0.060(5)
H	–0.146(4)	0.321(2)	–0.142(4)	0.18(3)*	0.07†
			***T* = 779 °C (hematite)**		
Fe	0	0	3.550(1)	11.41(4)	0.067(5)
O	0.313(1)	0	0.25	18	0.068(5)
H	–0.117(4)	0.324(2)	–0.143(4)	0.18(4)*	0.08

* Restricted to the chemical composition of protohematite (see text for details).
† Interpolated value from the literature.

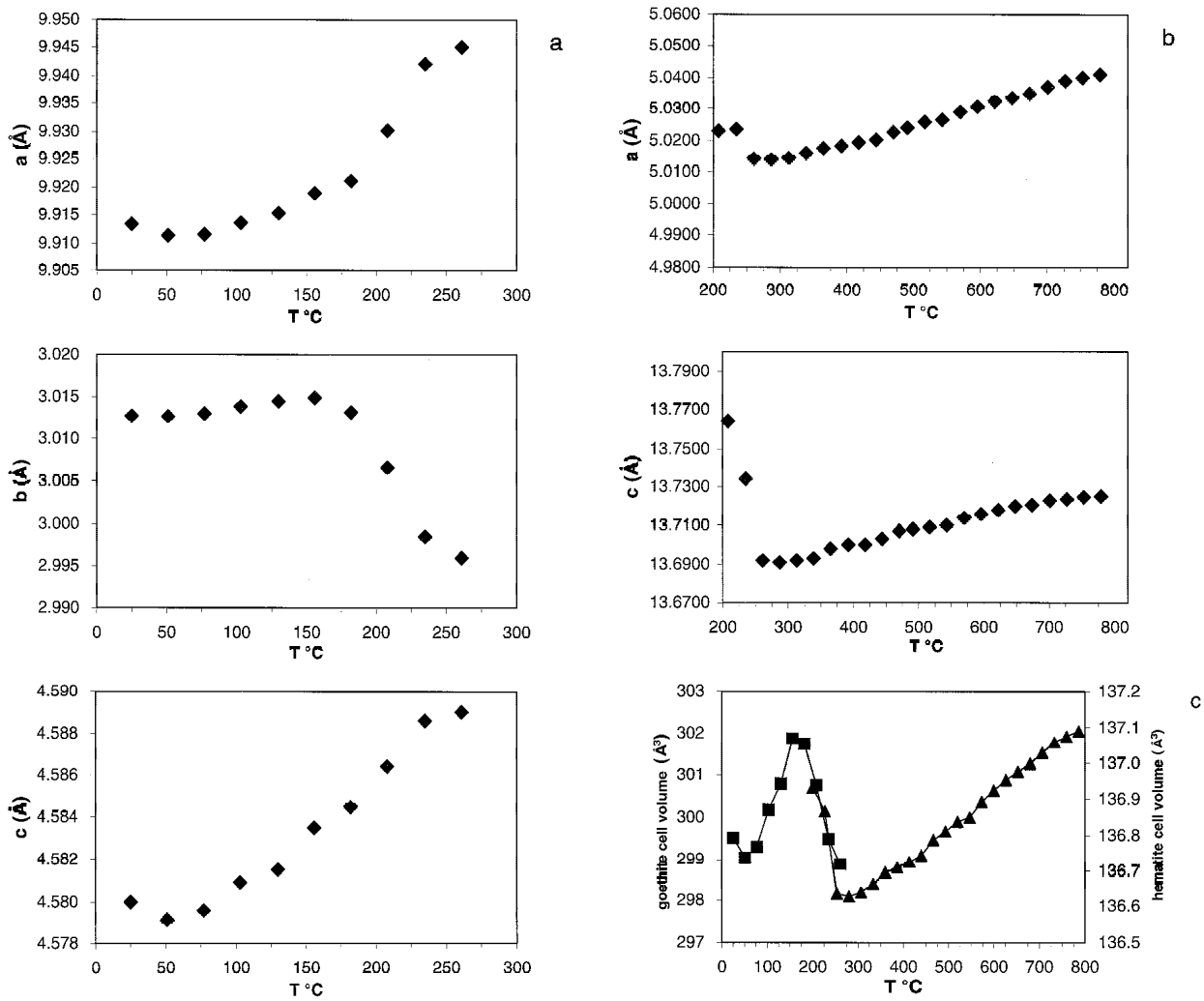

FIGURE 7. Evolution of the cell parameters with temperature for **(a)** goethite, **(b)** hematite, and **(c)** compared cell volume for both phases with full squares = goethite, full triangles = hematite. Standard deviations are smaller than drawn points.

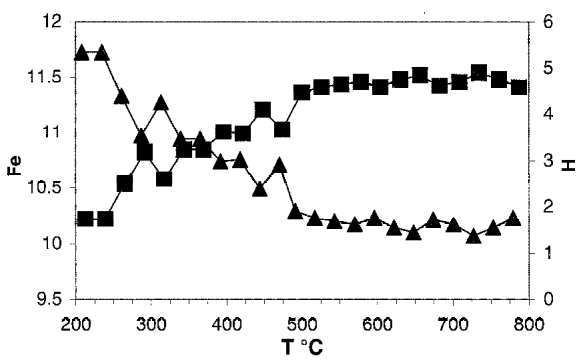

FIGURE 8. Changes in the refined iron population (full squares) and restrained hydrogen population (full triangles) with temperature in protohematite. Standard deviations are smaller than drawn points. See text for details.

water loss, the stoichiometry FeOOH was achieved.

Concerning the behavior of the sample before the phase transformation, it was observed that the parameters of the pseudo-Voigt function were roughly constant and the Gaussian coefficient GU, which is proportional to the microstrain broadening was constantly refined to values about zero. This ruled out the behavior described by Koch et al. (1986) in which the increasing desorption of water leads to an increase in microstrain and to an enhanced magnetic coupling between neighboring microcrystals, giving rise to the so called superferromagnetic behavior. A decrease of the size of the crystallites with temperature was also ruled out because the Lorentzian coefficient LX was roughly constant until 200 °C. Refinement of the site populations did not show any variation. Thus, before the phase transformation, neither loss of protons nor microstructure variations of the sample were observed. Thermal expansion of the unit cell was observed until the phase transformation, especially along the *c* axis, with a relaxation of the octahedra toward the empty cavities as evidenced by the

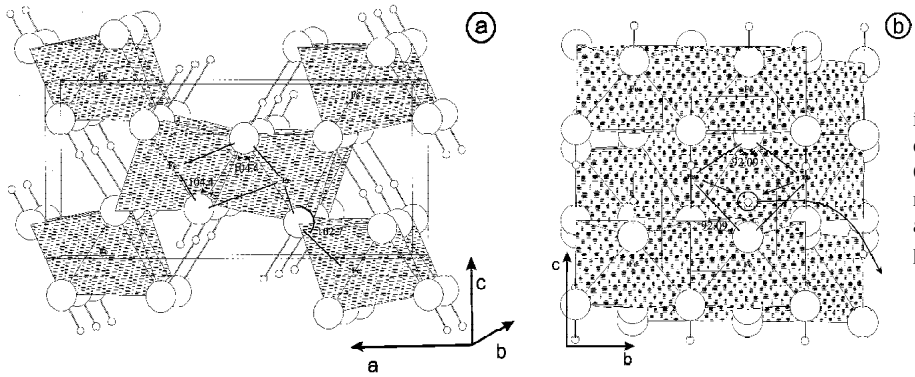

FIGURE 9. Structure deformations in goethite with temperature before the decomposition. Large empty circles are O atoms, small empty circles are residual protons. **(a)** projection in the a-c plane; **(b)** projection in the b-c plane. See text for details.

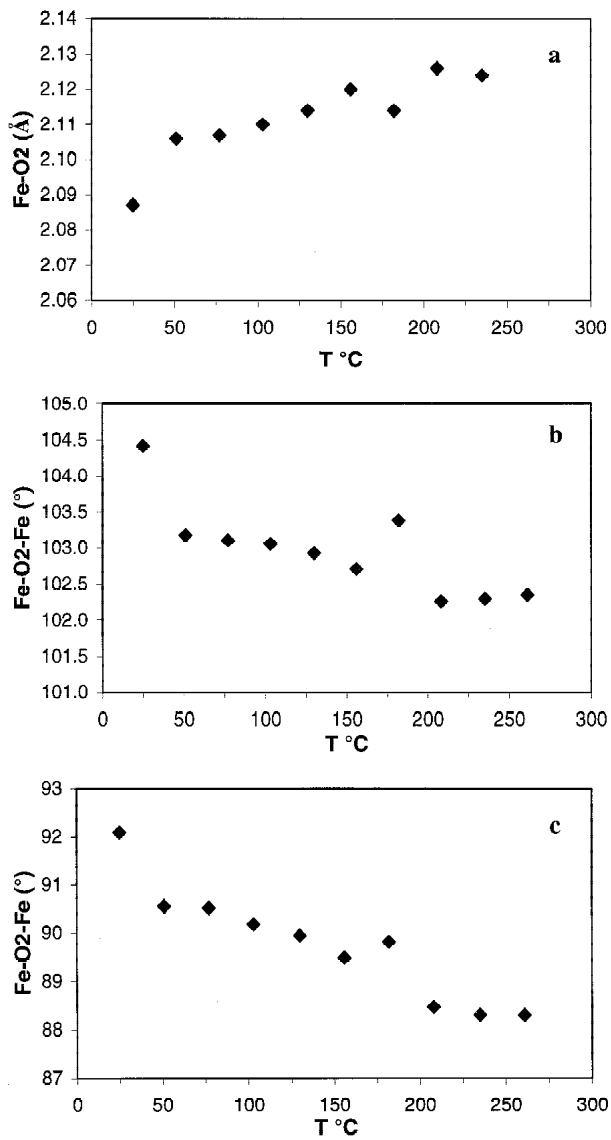

FIGURE 10. Distances and angles variation in goethite before the decomposition: Fe-O_2 distance **(a)**; Fe-O_2-Fe angle between edge sharing octahedra **(b)** and between adiacent octahedra along *b* **(c)**. Standard deviations are smaller than drawn points. See text for details.

shift of O_2 atoms of the same octahedral edge in opposite directions (Figs. 9a and 9b). Consequently the Fe-O_2 distance increased (Fig. 10a) and the Fe-O_2-Fe angles between edge sharing octahedra and between adiacent octahedra along *b* (Figs. 10b and 10c) decreased. No variations in the O_2-proton distance was observed before the transformation.

The decomposition of goethite started at 200 °C and concluded at about 270 °C. During the transformation, a dramatic decrease of *b* was observed and determined the volume contraction while *a* and *c* expanded. This is due to the relaxation around the vacancy generated by the proton migration from the structure. O_1 and O_2 moved in opposite directions (Fig. 9b) and Fe atoms moved closer along the *b* direction. Consequently the Fe-O_1-Fe and Fe-O_2-Fe angles decreased. The structure of phase formed from the decomposition of goethite was a non-stoichiometric hematite which can be described as "protohematite" $Fe_{2-x/3}(OH)_xO_{3-x}$ (Wolska and Schwertmann 1989). Protons were retained for charge balance since the structure was defective in iron (three H atoms were retained for each Fe atom deficiency). The structure refinement thus confirmed the occurrence of this intermediate non-stoichiometric phase in the sequence goethite-hematite albeit in our sample $x = 0.88$ at 235 °C that was in slight disagreement with the value reported by Wolska and Schwertmann (1989): $x = 0.97$ at 250 °C. This model was also in agreement with the IR spectra by Kustova et al. (1982) showing characteristic absorption bands of OH groups until 900 °C. During the phase transformation, the migration of protons and hydroxyls was related to a migration of Fe atoms along *c*, which reordered to form hexagonal rings typical of hematite. Because iron occupied one-half of the octahedral cavities in goethite and two-thirds in hematite, the mass balance was fulfilled by the formation of an Fe-defective hematite. The way migration and reordering occurred was random albeit two ordering schemes with reciprocal orientation relationships were likely favored (layers a and b in Fig. 11). They were the obverse and reverse twin settings described by Lima de Faria (1963) and Watari et al. (1979b). Powder diffraction is not capable of detecting twinning and thus cannot rule out the existence and the extent of the twinned domains in protohematite. However, a clear indication of disorder was given by the anisotropic broadening of peak profiles in protohematite indicating that a partially destructive interference due to a defective distribution of Fe atoms and residual protons. Such a disorder was observed by Lima de Faria (1963) and could be described as planar stacking defectiveness with

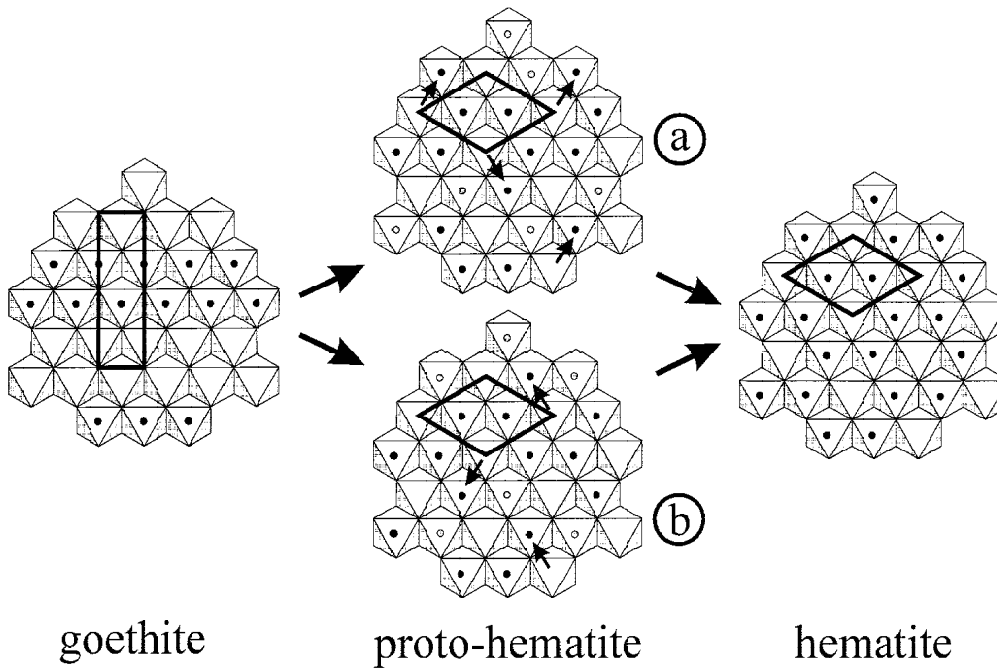

FIGURE 11. The two most probable ordering schemes of iron during the goethite-protohematite phase transformation and final transformation to hematite.

broadening affecting all the reflections that do not obey the *h-k* = 3*n* and *l* = 3*n* conditions, indicating a sub-cell (original goethite) with a different base and a height one third of the normal hexagonal cell. Thus, the overall iron defectiveness in protohematite yielded a lower refined site population, and the destructive interference effects given by the disordered iron distribution or faulted stacking sequence induced an anisotropic peak broadening simulated by specific profile parameters of the pseudo-Voigt.

Regarding the kinetics of the process, Goss (1987) showed that the reaction starts at the surface of goethite and proceeds inward with the formation of empty layers (pores) perpendicular to the *c* axis. The rate-limiting step was an interface reaction process and not long-range diffusion. This was in agreement with a model where iron locally reorders and concentrates in layers. Goss (1987) also observed a partial diffusive control on the reaction in its initial steps and this also was consistent with an initial long-range migration of hydroxyls and protons out of the structure along the cavities of the *b* axis.

This scenario was well consistent with the results of the thermal analysis showing a double peak either in the DTA and the DTG data corresponding to the goethite-protohematite phase transformation. The first peak was due to the reaction enthalpy necessary for the earlier long-range diffusion of hydroxyls and protons along the cavities of the *b* axis, which is significant only in samples with large-grain size. In fact, Schwertmann et al. (1985) observed that the larger the grain size, the larger the area of the first peak. Colloidal samples eventually do not show that peak. The second peak was due to condensation of H_2O

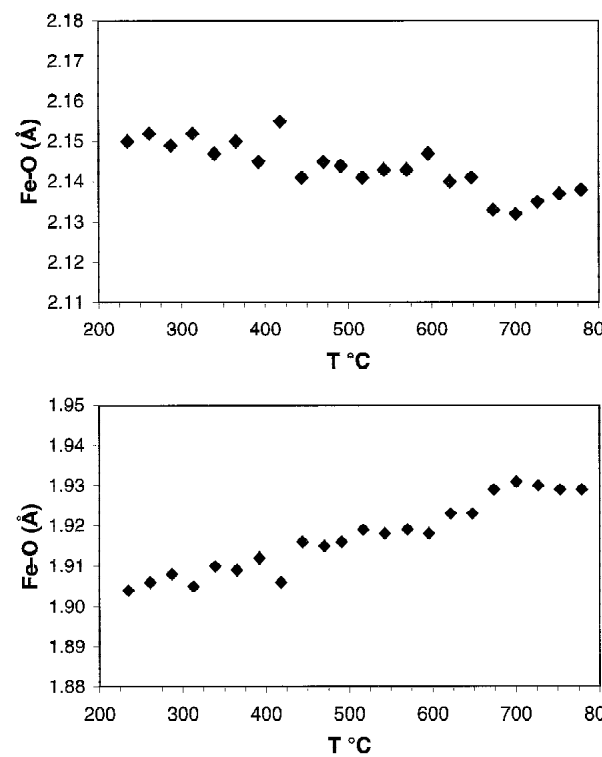

FIGURE 12. Variation of the non equivalent Fe-O distances with temperature. Standard deviations are smaller than drawn points. See text for details.

molecules and expulsion in the reacting goethite as a consequence of the migration along *c* and redistribution of Fe atoms. The reaction proceeded inward as the Fe migrates leaving clusters of residual protons and O atoms, which condensated into H_2O molecules that were released. In agreement, TG showed a continuous loss of weight after the phase trasformation goethite-protohematite up to 800 °C.

After the phase transformation, the decrease of the LY, sfec, and ptec coefficients with temperature meant that protohematite formed by Fe-deficient layers with residual protons progressively reordered in temperature, that is iron concentrated in ordered hematite clusters. Residual protons and O atoms instead concentrated in empty layers, condensated into H_2O molecules subsequently expelled from the material, leaving pores, as observed by Watari et al. (1979a). In concert with this, there was a clear correlation between the decrease of the sfec profile coefficient, simulating the stacking fault defectiveness, and the increase of iron population in hematite (and consequently the restrained decrease of the population of hydrogen). Linear regression of sfec against iron (or hydrogen) population in protohematite yielded a coefficient of 0.93. Thus, at high temperature, protohematite transformed in porous hematite.

A continuous increase of hematite *a* and *c* axes (thermal expansion) was observed and was not in agreement with Wolska and Schwertmann (1989) who reported an increase of *a* and a decrease of *c* with temperature. Two reasons may be invoked to explain this difference: (1) their samples had a different microstructure and thus were not directly comparable with our sample (it is a bit surprising that the authors intentionally omitted to report the data for sample no. 10, which seems to be very similar to our sample); (2) it was possible that thermal expansion concealed a decrease of the *c* cell dimension (which was more or less invariant in their ex situ data). Two contemporary trends may occur: a decrease of *c* due to the loss of protons and an increase due to thermal expansion, the latter prevailing and leading to the observed trend.

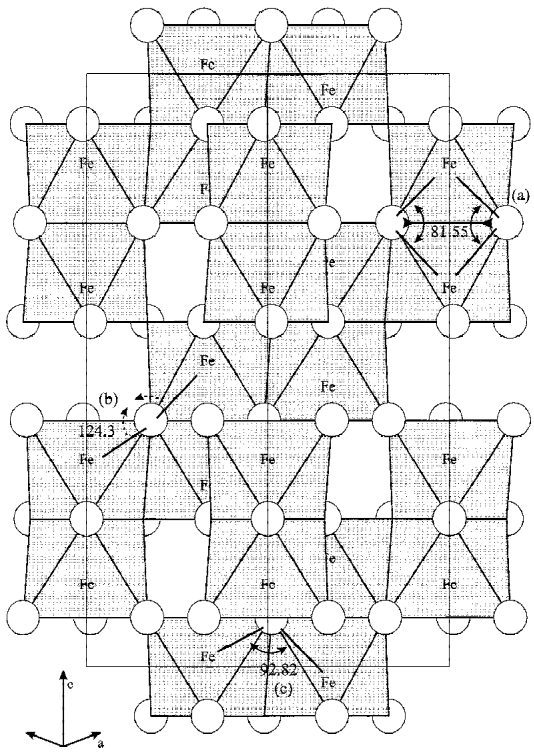

FIGURE 13. The structure deformations in protohematite with temperature. Large empty circles are O atoms. Residual protons are not depicted for the sake of clarity. Full black arrows mean that the angle is increasing, dashed arrows mean that the angle is decreasing. The situation **(a)** shows the increase of the Fe-O-Fe angle involving iron atoms of face sharing octahedra and the oxygen laying on that face (see relative Fig. 14a); situation **(b)** shows the decrease of the Fe-O-Fe angle involving iron atoms belonging to corner sharing octahedra (see relative Fig. 14b); situation **(c)** shows the increase of the Fe-O-Fe angle involving iron atoms belonging to edge sharing octahedra (see relative Fig. 14c).

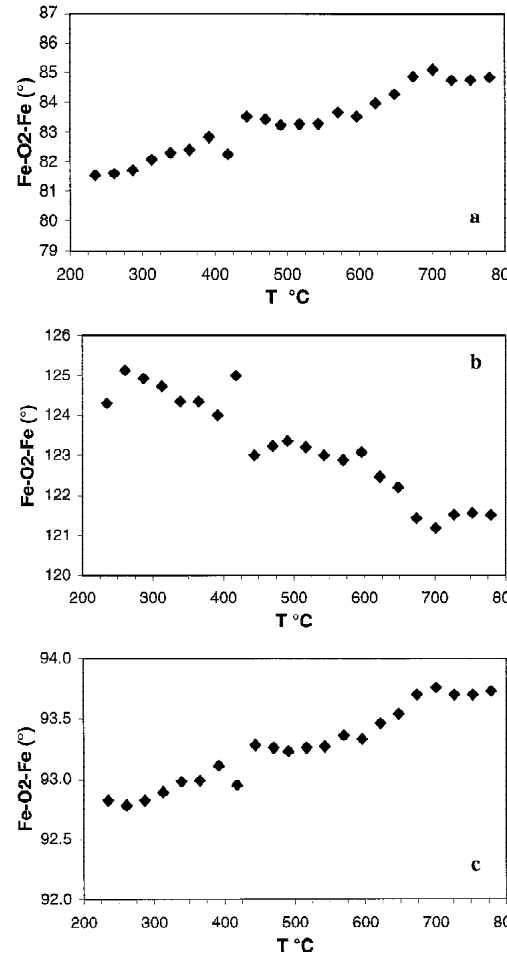

FIGURE 14. Distances and angles in protohematite with temperature: **(a)** Fe-O-Fe angle involving iron atoms of face sharing octahedra and the oxygen laying on that face; **(b)** Fe-O-Fe angle involving iron atoms belonging to corner sharing octahedra; **(c)** Fe-O-Fe angle involving iron atoms belonging to edge sharing octahedra. Standard deviations are smaller than drawn points. See text for details.

The progressive loss of protons in protohematite induced a symmetrization of the geometry of the octahedra because the O atoms moved closer to the coordinated Fe atoms to balance for the loss of the proton positive charge (see the decrease of the Fe-O distance with temperature in Figs. 12a and 12b).

The processes of deprotonation and Fe migration to form complete hematite layers were certainly responsible for the distortion of adjacent face-sharing octahedra. It was observed that the O atoms of face-sharing octahedra had a tendency to move toward the center of the face with a minimization of the shared area and consequently a minimization of the lattice energy. The relative modification of the structure depicted in Figure 13 resulted from the following changes with temperature: increase of the Fe-O-Fe angle involving iron atoms of face sharing octahedra and the oxygen laying on that face (Fig. 14a); decrease of the Fe-O-Fe angle involving Fe atoms belonging to corner-sharing octahedra (Fig. 14b); increase of the Fe-O-Fe angle involving Fe atoms belonging to edge-sharing octahedra (Fig. 14c).

Finally, at 800 °C, the temperature reached with our experiment, protohematite was almost completely converted to hematite.

ACKNOWLEDGMENTS

The present research is supported under contract DE-AC02-98CH10886 with the U.S. Department of Energy by its Division of Chemical Sciences, Office of Basic Energy Sciences. A.F.G. acknowledges funding from Italian MURST and CNR and benefited a grant from Fullbright U.S.A.-Italy cultural exchange commission. J. Hanson is greatly acknowledged as X7B beam line responsible and for reading the manuscript. T. Giliberti is acknowledged for the thermal analysis. Thanks are due to the referees (J. Rakovan and an anonymous one) for the careful revision and improvement of the manuscript.

REFERENCES CITED

Amemija, Y. (1990) Imaging Plate-X ray area detector based on photostimulable phosphor. Synchrotron Radiation News, 3, 21–26.

Bernal, J.D., Dasgupta, D.R., and Mackay, A.L. (1958) The oxides and hydroxides of iron and their structural interrelationships. Clay Minerals Bullettin, 4, 15–30.

Blake, R.L., Hessevick, R.E., Zoltai, T., and Finger, L.W. (1966) Refinement of the hematite structure. American Mineralogist, 51, 123–129.

Cagliotti, G., Paoletti, A., and Ricci, F.P. (1958) Choice for collimators for a crystal spectrometer for neutron diffraction. Nuclear Instruments, 3, 223–228.

Francombe, M.H. and Rooksby, H.P. (1959) Structure transformation effects by the dehydration of diaspore, goethite, and delta ferric oxide. Clay Minerals Bullettin, 4(21), 1–14.

Goldsztaub, S. (1931) Deshydratation des hydrates ferriques naturales. Comptes Rendus de la Academie Science Paris, 193, 533–535.

Goss, C.J. (1987) The kinetics and reaction mechanism of the goethite to hematite tranformation. Mineralogical Magazine, 51, 437–51.

Gualtieri, A.F., Norby, P., Hanson, J., and Hriljac, J. (1996) Rietveld refinement using synchrotron X-ray powder diffraction data collected in transmission geometry using an Imaging Plate Detector: application to standard *m*-ZrO_2. Journal of Applied Crystallography, 29, 707–713.

Hastings, J.B., Suortii, P., Thomlinson, P., Kvick, Å., and Koetzle, T. (1983) Optical design for the NSLS crystallography beam line. Nuclear Instruments and Methods, 208, 55–58.

Hoppe, W. (1940) Über die Kristallstruktur von α-AlOOH (Diaspor) und α-FeOOH (Nadeleisenerz). Zeitschrift für Kristallographie, 103, 73–89.

Koch, C.J.W., Madsen, M.B., Mørup, S., Christiansen, G., Gerward, L., and Villadsen, J. (1986) Effect of heating on microcrystalline synthetic goethite. Clays and Clay Minerals, 34, 17–24.

Kustova, G.N., Burgina, E.B., Sadykov, V.A., and Poryvaev, S.G. (1982) Vibrational spectroscopic investigation of the goethite thermal decomposition products. Physics and Chemistry of Minerals, 18, 379–382.

Langford, J.I., Boultif, A., Auffredic, J.P., and Louër, D. (1993) The use of pattern decomposition to study the combined X-ray diffraction effects of crystallite size and stacking faults in ex-oxalate zinc oxide. Journal of Applied Crystallography, 26, 22–23.

Larson, A.C. and Von Dreele, R.B. (1998) GSAS. General Structure Analysis System. Report LAUR 86-748. Los Alamos National Laboratory, Los Alamos, New Mexico.

Lima-de-Faria, J. (1963) Dehydration of goethite and diaspore. Zeitschrift für Kristallographie, 119, 176–203.

Louër, D. and Langford, J.I. (1988) Peak shape and resolution in conventional diffractometry with monocromatic X-rays. Journal of Applied Crystallography, 21,430–437.

Norby, P. (1997) Syncrotron powder diffraction using imaging plates: crystal structure determination and Rietveld refinement. Journal of Applied Crystallography, 30, 21–30.

Palache, C., Berman, H., and Frondel, C. (1944) Dana's Systems of mineralogy. 7th edition, Wiley, New York.

Rooksby, H.P. (1951) Effect of heat-treatment on goethite and lepidocrocite. In G.W. Brindley, Ed., X-ray identification and crystal structures of clay minerals, p. 260–261. Mineralogical Society, London.

Schwertmann, U., Cambier, P., and Murad, E. (1985) Properties of goethites of varying crystallinity. Clays and Clay Minerals, 33, 369–378.

Szytuta, A., Burewicz, A., Dimitrijevic, Z., Krasnicki, S., Rzany, H., Todorovic, J., Wanic, A., and Wolski, W. (1968) Neutron diffraction studies of α-FeOOH. Physica Status Solidi, 26, 429–434.

Van Berkum, J.G.M., Delhez, R., de Keijser, Th.H., and Mittemeijer, E.J. (1996) Diffraction-line broadening due to strain fields in materials; fundamentals aspects and methods of analysis. Acta Crystallographica, A52, 730–747.

Watari, F., Van Landuyt, J., Delavignette, P., and Amelinckx, S. (1979a) Electron microscopic study of dehydration transformations. Part I: Twin formation and mosaic strusture in hematite derived from goethite. Journal of Solid State Chemistry, 29, 137–150.

Watari, F., Delavignette, P., and Amelinckx, S. (1979b) Electron microscopic study of dehydration transformations. Part II: The formation of "superstructures" on the dehydration of goethite and diaspore. Journal of Solid State Chemistry, 29, 417–427.

Watari, F., Delavignette, P., Van Landuyt, J., and Amelinckx, S. (1983) Electron microscopic study of dehydration transformation. Part III: High resolution observation of the reaction process $FeOOH \rightarrow Fe_2O_3$. Journal of Solid State Chemistry, 29, 49–64.

Wolska, E. (1981) The structure of hydrohematite. Zeitschrift für Kristallographie, 154, 69–75.

Wolska, E. and Schwertmann, U. (1989) Nonstoichiometric structures during dehydroxylation of goethite. Zeitschrift für Kristallographie, 189, 69–75.

Young, R.A. and Wiles, D.B. (1982) Profile shape functions in Rietveld refinements. Journal of Applied Crystallography, 15, 430–438.

MANUSCRIPT RECEIVED JUNE 29, 1998
MANUSCRIPT ACCEPTED DECEMBER 21, 1998
PAPER HANDLED BY JAMES W. DOWNS